Explotiong elastic energy storage for cyclic manipulation:
An analysis for basketball dribbling wit an anthropomorphic robot

Sami Haddadin, Kai Krieger, Mirko Kunze and Alin Albu-Schäffer

Abstract— **For creating robots that are capable of human like performance in terms of speed, energetic properties, and robustness, intrinsic compliance is a promising design element for achieving this. In this paper we investigate the effects of elastic energy storage and release for ball dribbling in terms of cycle stability based on the analysis of error evolution, peak power performance during hand contact, and robustness with respect to varying finger stiffness. As the ball can only be controlled during contact, an intrinsically elastic finger extends the contact time and the energetic characteristics of the process. As a human is able to dribble blindly, we decided to develop the foundation for the case of contact force sensing only, i.e. no vision is used for our approach.**

I. INTRODUCTION

Hybrid object manipulation has been investigated since many years. Robot dribbling as an example for this was first introduced in [1]. The authors used a half-cylindrical tube for mapping the system to a 2-D system. The control is reactive and pushes the ball only downwards if a contact is detected. [2] utilizes a high-speed multi-fingered hand for dribbling a ping-pong ball. This experiment was used for evaluating their high-speed vision for ball tracking. [3] introduced a basketball playing industrial robot, utilizing a solid plate as hand. The control mainly relies on the ball tracking vision system and achieves stability. In [4] the authors used an elastic element for lengthening the contact time and storing elastic energy in the system based on an optimal control trajectory.

Related to dribbling is the classical juggling task. [5] investigated this first. They use a mirrored and scaled version of the ball trajectory which means that the ball has to be tracked over the entire cycle. In [6] the first blindly juggling robot was presented. [7] used only a linear motor for juggling without the need of active ball tracking, as the lateral motion is stabilized by the shape of the juggling paddle. In [7] the authors compared an $\mathcal{H}_2$ optimal controller with the previous open-loop control, which turned out to have similar performance characteristics.

in this paper we present experiments of an elastic dribbling robot in 6 DoF, which is an interesting problem in order to further understand how intrinsic elasticity can be used to achieve high-performance and energy efficiency during highly dynamic and repetitive tasks like in throwing [8], walking [9] and batting [10]. Several questions arise when intrinsic elasticity is taken into account. A particular important one is how to select the spring stiffness for optimally achieving a given task. Our aim is to analyze this by considering the dribbling problem, as this poses high demands on the robot in terms of speed, dexterity, and robustness. A rather intuitive benefit why compliance is desired, which however has not been shown up to now, is that the robot should be able to sustain longer ball contact over a longer time period

The first two authors contributed equally to the work. S. Haddadin*, K. Krieger, Mirko Kunze and A. Albu-Schäffer are with the Institute of Robotics and Mechatronics, DLR - German Aerospace Center, Wessling, Germany, contact: `sami.haddadin@dlr.de`

compared to stiff robots. In turn, this should yield a better opportunity to robustly control the ball.

In [11] we analyzed therefore the stability of a 1 DoF system and also gave an observation method for tracking the ball based on measuring the contact forces only. Therefore, we also gave a stability analysis.

In this paper we extend the 1 DoF system to full 6 DoF for the ball in Sect. II. In Sect. III we extend the observer presented in [11] for the observation of all three translations and also add a control for the lateral motion of the ball. We end up this paper in Sect. IV by presenting measurements that we made with an human during basketball dribbling as well as simulations for a 3 DoF and 6 DoF ball model and also some experiments we have done on a real robot.

II. MODELING

Todo 1
- *conclusion*
- *Bild Hand Verena*
- *Bildsequenz dribbeln Verena*
- *Bewegungsgl. fr Simulation sami diss*

In this section we outline a model for the dribbling robot. For this, we have to describe two distinct bodies. One is the ball and the other is the hand of the robot. A schematic view of this is shown in Fig. 1. The robot flange with the spring as a finger is shown in the upper part of the picture. In reality we use three fingers that are located in one plane, cf. Fig. 2. The fingers are directly made of spring steel. For the damping of the impact we glued some foam material on them.
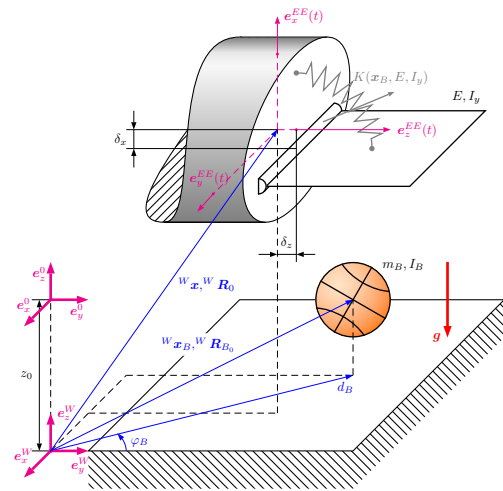

Fig. 1. Model of the overall model with robot and basketball.

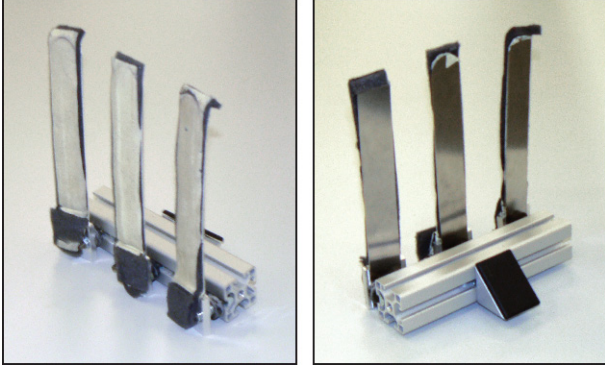In the modelling part, we use only one spring as a substitute, cf. Fig. 1. The basketball is located beneath it.

Fig. 2. Hand used for basketballdribbling.

Both bodies are described by their position vector and a rotation matrix. There are three different frames depicted. One is the end effector frame EE. The others are the world W, which is located on the floor and the base frame of the robot denoted by 0, which is located above the world frame. The mount of the spring is translated in the EE frame by the shown offsets δ_z and δ_x.

In the following we will first go into the detail of the ball model. Further on, we show how to obtain the forces acting on the ball. All vectors in the following will be in the W frame unless specified otherwise. Hence, we drop the index for the frame.

A. Ball model

The ball is modeled as a free body with a force $\boldsymbol{F}_B$ acting on its perimeter and a vector of weight force $\boldsymbol{g}$. Therefore, it is described by three translational coordinates $\boldsymbol{x}_B = [x_B \; y_B \; z_B]^T$, their velocities $\dot{\boldsymbol{x}}_B$ and the quaternion $\boldsymbol{q}_B = [q_0 \; q_1 \; q_2 \; q_3]^T$, and three rotational velocities $\boldsymbol{\omega}_B = [\alpha_B \; \beta_B \; \gamma_B]^T$ around the axes of the world frame. This yields

$$\begin{bmatrix} \ddot{\boldsymbol{x}}_B \\ \dot{\boldsymbol{q}}_B \\ \dot{\boldsymbol{\omega}}_B \end{bmatrix} = \begin{bmatrix} \frac{1}{m_B}\boldsymbol{F}_B + \boldsymbol{g} \\ \frac{1}{2}Q(\boldsymbol{q})\boldsymbol{\omega}_B \\ I_B^{-1}(\boldsymbol{r}_B \times \boldsymbol{F}_B) \end{bmatrix} \quad (1)$$

with $\boldsymbol{r}_B$ being the vector from the center of the ball to the force application point, m_B being the mass of the ball and I_B denoting the inertia tensor of the ball that is diagonal due to the ball's rotational symmetry. $Q(\boldsymbol{q})$ is a matrix that maps the Cartesian velocities to quaternion velocities, cf. [12]. The calculation of the force $\boldsymbol{F}_B$ is shown in the following paragraphs.

For the control presented later it is useful to have the translational coordinates also in cylindrical coordinates $\boldsymbol{x}_{BC} = [\varphi_B \; d_B \; z_B]^T$, see Fig. 1. Those are calculated via

$$\boldsymbol{x}_{B_c} = \begin{bmatrix} \varphi_B \\ d_B \\ z_B \end{bmatrix} = \begin{bmatrix} \arctan_2(-x_B, y_B) \\ \sqrt{x_B^2 + y_B^2} \\ z_B \end{bmatrix}. \quad (2)$$

B. Floor contact

The ball is in floor contact if

$$z_B \leq r_B \quad (3)$$

with r_B being the radius of the ball. The calculation of the contact force is split up into two components. $\boldsymbol{F}_{FC_n}$ the normal force and $\boldsymbol{F}_{FC_t}$ the force tangential to the floor plane.

1) Normal force: The normal force is calculated by a Hunt-Crossley Model [13] that is

$$\boldsymbol{F}_{FC_n} = \left(-K_F(z_B - r_B) - D_F(z_B - r_B)\dot{z}_B\right)\boldsymbol{e}_z \quad (4)$$

with K_F being the stiffness constant and D_F the damping constant.

2) Tangential force: The physical effect that arouses by the tangential force is that the relative velocity between ball and floor fades away over the contact due to the friction. This effect is taken into account by a lumped LuGre model [14] that is given by

$$\dot{s} = v_r - \frac{\sigma_0|v_r|}{g(v_r)}s \quad (5)$$

$$F = (\sigma_0 s + \sigma_1 \dot{s} + \sigma_2 v_r)F_n, \quad (6)$$

with

$$g(v_r) = \mu_C + (\mu_s - \mu_c)e^{-|v_r/v_s|^\alpha}. \quad (7)$$

Thereby σ_0 is the rubber longitudinal lumped stiffness, σ_1 the rubber longitudinal lumped damping, σ_2 the viscous relative damping, μ_c the normalized Coulomb friction, μ_s the normalized static friction, v_s the Stribeck relative velocity, F_n the normal force, v_r the relative velocity and s the internal friction state. The steady-steady friction/slip characteristic is captured by α.

The relative velocity is calculated by

$$\boldsymbol{v}_{FC_r} = [\boldsymbol{0} \; \boldsymbol{e}_y \; \boldsymbol{e}_z]\dot{\boldsymbol{x}}_B + [0 \; 0 \; -r_B]^T \times \boldsymbol{\omega}_B. \quad (8)$$

(8) provides also the direction of the tangential force, as it acts opposite to the direction of the relative velocity.

C. Hand model

The robot end effector is commanded via a rotation matrix and the position vector in Cartesian impedance control. The rotation matrix is described by a set of Euler angles, whose rotation order is shown in Fig. 3.
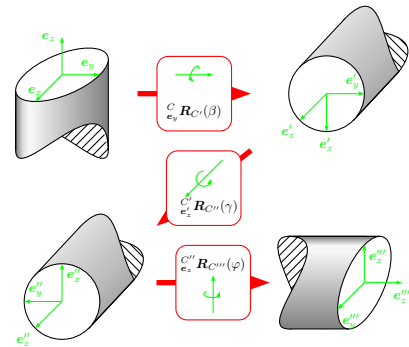

Fig. 3. Rotation order of the robot hand.

The first coordinate system C is collinear to the base frame. The first rotation acts around the y-axis and is later used for the control of the ball along the d_B coordinate. Thereafter, the coordinate system is rotated around the new z-axis which will be used for control of the ball along the φ_B coordinate. The last rotation is around the z-axis of the base frame and is used for tracking the ball position.

D. Hand contact

The hand contact is calculated similar to the floor contact. Therefore it is advantageous to use the position vector of the ball expressed in the end effector frame. The condition for hand contact is

$$x_B^{EE} \geq \delta_x + r_B. \tag{9}$$

We assume that there is no damping in the hand as the fingers are made of spring steel. Hence we get

$$\boldsymbol{F}_{HC_n} = K(\boldsymbol{x}_B, E, I_y)(-x_B^{EE} + \delta_x + r_B)\boldsymbol{e}_x^{EE} \tag{10}$$

for the normal direction of the contact. The stiffness $K(\boldsymbol{x}_B, E, I)$ is calculated from the linear theory on Bernoulli beams, Fig. 4. The force F denotes the force that is applied by the ball. Hence, we get the two reactions M_R and N. We also get the sketched bending line $w(z)$, which is calculated by [15]

$$EI_y \frac{\mathrm{d}^2 w(z)}{\mathrm{d}z^2} = -M_y(z), \tag{11}$$

with E as the modulus of elasticity, I_y as the geometrical moment of inertia around the y-axis and M_y as the bending moment diagram around y, which is obtained as

$$M_y(z) = \underbrace{Fz_F}_{=M_r} - \underbrace{F}_{=N}z + \begin{cases} 0 & \text{for } z \leq z_F \\ F(z - z_F) & \text{for } z > z_F \end{cases}. \tag{12}$$
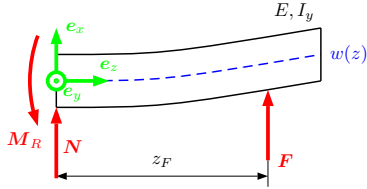

Fig. 4.   Calculation of spring stiffness.

By evaluating (11) at z_F we obtain a relation between the force and the bending at z_F as

$$F = \underbrace{\frac{EI_y}{3z_F^3}}_{K} w(z_F). \tag{13}$$

Therewith the stiffness is known. The tangential direction of the force is calculated analogue to Sect. II-B by utilizing a LuGre model.

In the next section we will give an overview on the extension of the ball observer for three translational motions and also how we control the ball.

III. CONTROL

Our aim is to dribble blindly with force feedback only. Thus, we have to observe the ball position. This is presented in the following. After that we show how the ball is controlled by the robot hand.

A. Observer

In the present work we want to track the ball by the force measurement in the hand only. Therefore, we use a 6 DoF force torque sensor mounted in the wrist of the robot. In the signal we obtain from this sensor also other signal parts apart from the contact force are contained. These signals are high frequency noise, an oscillation that is founded in the springs from the fingers, and also a force due to the acceleration of the hand mass. To eliminate the noise we filter the signal by a PT2 element. As the finger oscillation has only a small amplitude and the associated frequency is very close to the frequency spectrum of the contact force, we do not further treat it. As we are having fast accelerations on the robot the main contribute is the force due to the load acceleration. To filter it out we use a velocity disturbance observer for the robot to obtain the accelerations at the robot flange.

Todo 2
Verweis Sami Haddadin Dissertation

Suppose we got the equations of motion for an n-link manipulator as

$$\ddot{\boldsymbol{q}} = M^{-1}(\boldsymbol{\tau}_J - \boldsymbol{\tau}_{ext} - \boldsymbol{n}(\boldsymbol{q}, \dot{\boldsymbol{q}})). \tag{14}$$

with $\boldsymbol{q}$ as the joint angles, M as the mass matrix, $\boldsymbol{\tau}_j$ as the torques from the motors, $\boldsymbol{\tau}_{ext}$ as the external torques, and $\boldsymbol{n}$ as a vector consisting of gyroscopic and Coriolis terms.

The observer proposed in HADDADIN is then

$$\hat{\ddot{\boldsymbol{q}}} = M^{-1}(\boldsymbol{\tau}_J - \hat{\boldsymbol{n}}(\boldsymbol{q}, \dot{\boldsymbol{q}}) - K_O(\hat{\dot{\boldsymbol{q}}} - \dot{\boldsymbol{q}})) \tag{15}$$

with $\hat{\boldsymbol{q}}$ as the observed joint angles and K_O as the observer gains. In fig. 5 the block diagram of this observer is shown.
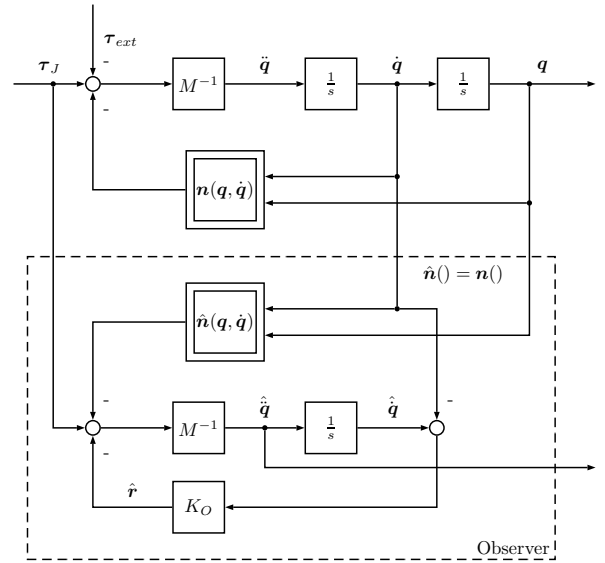

Fig. 5.   Velocity disturbance observer.

With the joint accelerations we easily obtain the Cartesian accelerations and consequently also the forces due to the accelerations via

$$\hat{\ddot{\boldsymbol{x}}} = \dot{J}\hat{\dot{\boldsymbol{q}}} + J\hat{\ddot{\boldsymbol{q}}}, \tag{16}$$

with J being the EE Jacobian of the manipulator. Therewith, we can subtract the forces due to the acceleration from the measured force signal.

In [11] we show how a nonlinear sliding mode observer can be set up for the observation of the vertical ball motion. The other translations x_B and y_B can be observed by a similar hybrid observer consisting of a sliding mode observer, cf. [16], in the hand contact and a prediction in the remaining non-contact phase.

For the observer part we need to achieve the position of the ball from the measured force. Therefore, we take advantage of the fact that at the point of contact only forces are acting on the hand and no torques. Thus, we use the principle of solidification. In this solid system there has to be a straight on which there are no moments acting [17]. This straight can be found by solving the equation

$$^{EE}\boldsymbol{M}_m = {}^{EE}\boldsymbol{r}_C \times {}^{EE}\boldsymbol{F}_m \qquad (17)$$

for $^{EE}\boldsymbol{r}_C$ which is the position vector of the point of contact. $^{EE}\boldsymbol{M}_m$ are the measured torques and $^{EE}\boldsymbol{F}_m$ are the measured forces. With $^{EE}\boldsymbol{r}_C$ and (4) we obtain the stiffness at the point of contact. Hence, with the direction of the straight, which is given by $^{EE}\boldsymbol{F}_m$ we get the ball position for the observer as

$$^{EE}\boldsymbol{r}_B = {}^{EE}\boldsymbol{r}_C + \frac{^{EE}\boldsymbol{F}_m}{|^{EE}\boldsymbol{F}_m|}\left(-r_B + \frac{|^{EE}\boldsymbol{F}_m|}{K(^{EE}\boldsymbol{r}_C, E, I_y)}\right),$$
$$(18)$$

which takes the radius r_B of the ball and the bending of the spring into account. As the sliding mode observer tends to scattering, we filter the observed ball position signal by a PT3 element before using it for a control.

B. Control

We want to stabilize the ball at a steady point $\boldsymbol{x}_{B_{des}}$. For the vertical motion we refer to [11], where a proof for the stability of the vertical motion with a sine like trajectory for the hand is given. Hence, the reference trajectory for the motion in z-direction is taken as granted. In this paper we want to take the vertical motion of the ball into account for which a stability analysis is still to be done.

The first thing for stabilizing the lateral motion is to follow the ball position with the hand position. For this, we use the position calculated in the ball observer in Sect. III-A. As we want to control the ball in the cylindrical coordinates depicted in Fig. 1, we get

$$\begin{bmatrix} x_{des} \\ y_{des} \\ \varphi_{des} \end{bmatrix} = \begin{bmatrix} -(d_B - \Delta_H) - \sin(\varphi_B) \\ (d_B - \Delta_H)\cos(\varphi_B) \\ \varphi_B \end{bmatrix} \qquad (19)$$

with Δ_H as an offset from the EE coordinate system to the middle of the finger.

Further on we want to attract the ball to $\boldsymbol{x}_{B_{des}}$. In order to achieve this we use a simple PID control for the two remaining rotations of the hand, which is given as

$$\beta_{des} = K_{P\beta}(d_{B_{des}} - d_B)$$
$$+ K_{I\beta}\int_0^t (d_{B_{des}} - d_B)\mathrm{d}\,d_B \qquad (20)$$
$$+ K_{D\beta}(\dot{d}_{B_{des}} - \dot{d}_B),$$

$$\gamma_{des} = K_{P\gamma}(\varphi_{B_{des}} - \varphi_B)$$
$$+ K_{I\gamma}\int_0^t (\varphi_{B_{des}} - \varphi_B)\mathrm{d}\,\varphi_B \qquad (21)$$
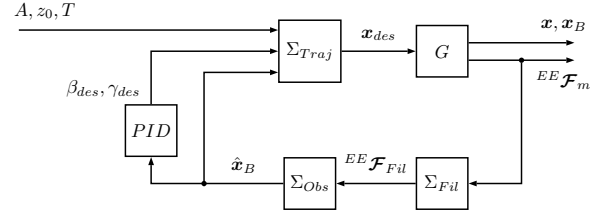$$+ K_{D\gamma}(\dot{\varphi}_{B_{des}} - \dot{\varphi}_B),$$

Fig. 6.   Control structure.

with K_{xx} being the respective gains for the PID control.

The overall structure of the closed loop system is shown in fig. 6. $A, z_0 and T$ are the given parameters for the z-axis trajectory, cf. [11]. G denotes the model of the robot and the ball and has the force wrench of the contact $^{EE}\boldsymbol{\mathcal{F}}_m = [^{EE}\boldsymbol{F}_m^T \ \ ^{EE}\boldsymbol{M}_m^T]^T$ and the position of the robot $\boldsymbol{x}$ as measured outputs. $^{EE}\boldsymbol{\mathcal{F}}_m$ is filtered in Σ_{Fil}. This filtered signal $^{EE}\boldsymbol{\mathcal{F}}_{Fil}$ is used in the observer Σ_{Obs} to construct the estimate of the position $\hat{\boldsymbol{x}}_B$, which is then used in the control laws given by (20) and (21).

IV. SIMULATIONS AND EXPERIMENTS

In the following section we first want to present some measureeent data we achieved by tracking a human during dribbling. Further on we want to show some results we achieved by using the model from II and III for a simulation. This section ends with some measurement we obtained in an experiment.

A. Measurement of a human.

By utilizing a Vicon tracking system running at 180 Hz and eight cameras we made measurements of a human playing basketball. Figure 7 depicts the positions of the tracked marker. Furthermore, the marker of the ball have been placed so that the position and the rotation of the ball could be tracked also when some marker were hidden by the hand during hand contact. In fig. 8 a sample configuration of the tracked data is shown. In Fig. 9 we show a sample
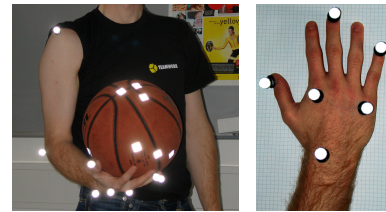

Fig. 7.   Setup and makrer position for the tracking.

of the measured data for the ball and three marker of the hand. Interesting is that the hand makes besides the vertical motion also a rotation araound the radial axes of the hand. Therefore, it can be seen in the lower velocity plot that the Wrist and the knuckle of the middle finger stops accelerating at the end of the contact and the fingertip is leading the ball further. Though, most of the downward ball speed is inserted by the fingers.

The fact of the rotation can also be seen in Fig. 10. The points of one pose from top to bottom are shoulder, ellbow, wrist, knuckle of middle finger and tip of middle finger.
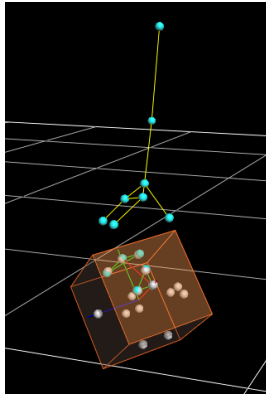
Fig. 8.   Sample Data of a tracked pose visualized in ViconIQ.
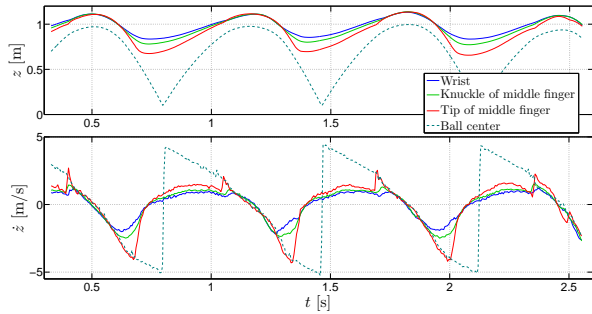

Fig. 9.   Measurement of Position and velocity for a sample dribbling measurement of a semi-pro human player.

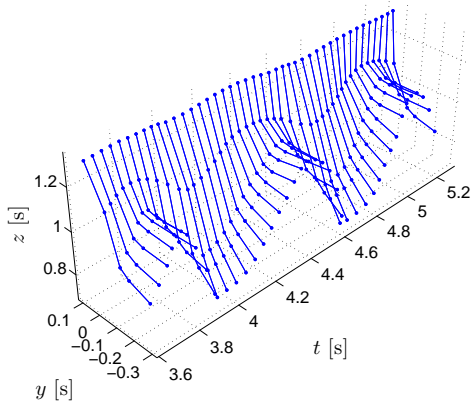Hence, we can see that the two lowest lines which are the palm and the finger are rotating.

Fig. 10.   Measurement of the pose for a sample dribbling measurement of a semi-pro human player.

B. Simulation with a 3 DoF ball.

For first simulations of the model in section II we locked the translations in x direction and the rotations about the y and z axis. In Fig. 11 we give a sample of this simulation. In the upper plot is the lateral position depicted. The steady state point of the ball is therefore at 0. The hand is measured at its EE coordinate system. Though we get the shift of the

hand to the ball because of the length of the finger. It can be seen that the ball is stabilized at zero. In the lower plot the vertical position is depicted. Also in this direction we obtain a stable cycle for the ball motion. Further we see that the observer is converging in two cycles towards the simulated ball trajectory.
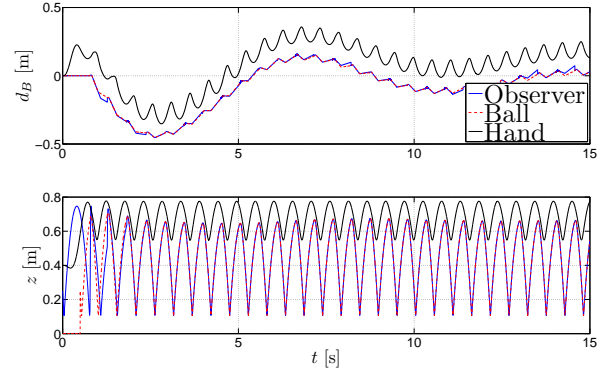

Fig. 11.   Position for a simulation with an 3 DoF ball.

C. Simulation with a 6 DoF ball.

Further we made simulations with the full model. In Fig 12 we depict therefore the position of the ball and the hand in the world coordinate system. We obtain the same offset on the y-axis as in the simulations with 3 DoF. We get therefore stable trajectories for the ball in all three axes.
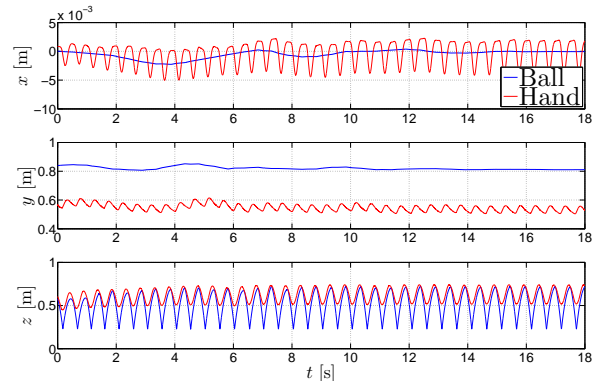

Fig. 12.   Position for a simulation with an 6 DoF ball.

Further in Fig. 13 we depict the forces that are used for observing the ball and are measured in the EE coordinate system. We get a maximal force of about 20 N during contact in the x-axis. the relative high force in the z-axis is caused by the friction of the ball.

D. Experiments.

We also made some experiments. A sample of the measurements obtained by the experiment can be seen in the figures 14 and 15. In the first figure the position of the ball in the cylindrical coordinates d_B and φ_B is shown.

In the second figure we find the measured and filtered forces. The maximal force in the upper plot is in a similar dimension as in the 6 DoF simulation (cf. fig. 13). In this plot it can be also seen the oscilation of the finger.
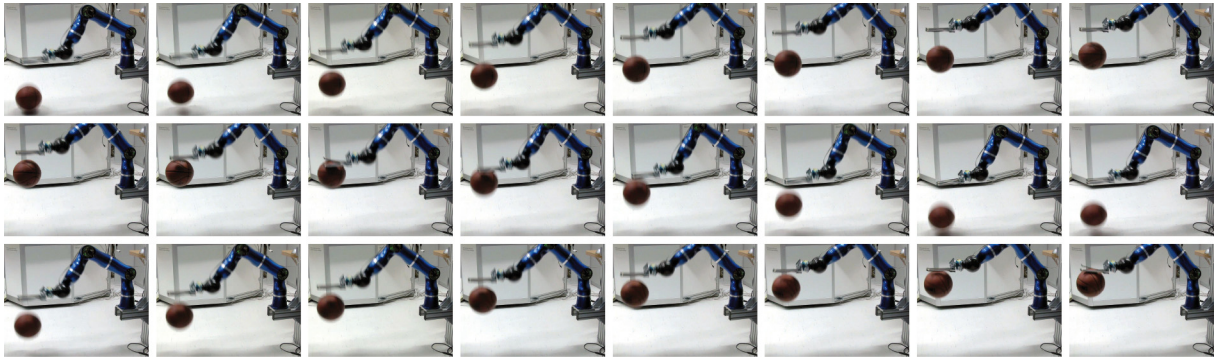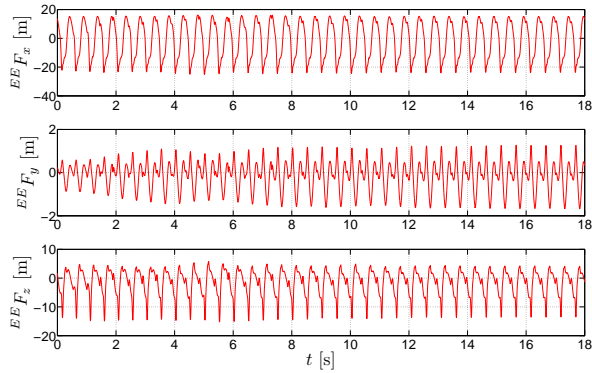
Fig. 16. Snapshots form basketball dribbling.
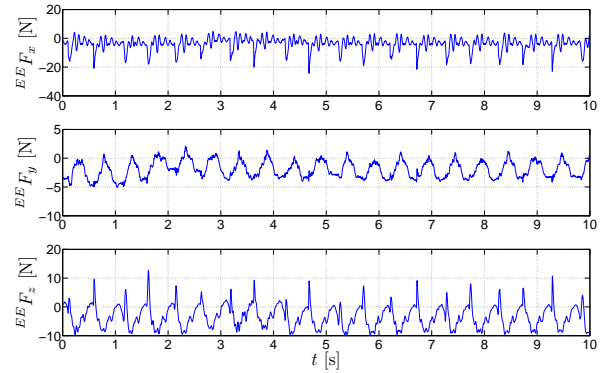

Fig. 13. Forces for a simulation with an 6 DoF ball.
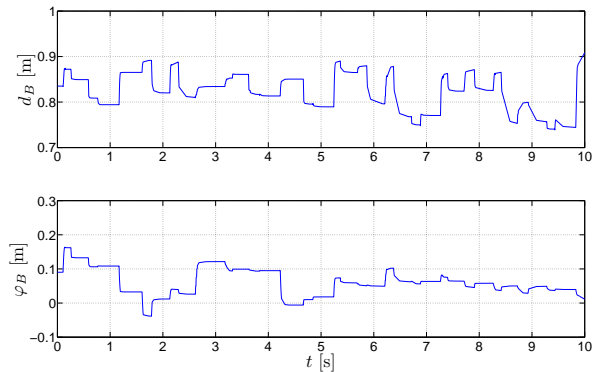

Fig. 15. Experiment force x.

Fig. 14. Experiment Position.

V. CONCLUSIONS

VI. ACKNOWLEDGMENTS

REFERENCES

[1] M. Stilman. (without date) Mike stilman: Previous projects. Visited on 28th of february 2011. [Online]. Available: http://www.cc.gatech.edu/ mstilman/earlier.html

[2] D. Shiokata, A. Namiki, and M. Ishikawa, "Robot dribbling using a high-speed multifingered hand and a high-speed multifingered hand and a high-speed vision system," in *2005 IEEE International Conference on Intelligent Robots and Systems*, Edmont, Canada, 2005, pp. 3945 – 3950.

[3] G. Bätz, M. Sobotka, D. Wolherr, and M. Buss, "Robot basketball: Ball dribbling - a modified juggling task," in *2008 IEEE International Conference on Robotics and Automation*, San Diego, USA, 2009, pp. 2410 – 2415.

[4] U. Mettin, A. S. Shiriaev, G. Bätz, and D. Wolherr, "Ball dribbling with an underactuated continuous-time control phase," in *2010 IEEE International Conference on Robotics and Automation*, Anchorage, USA, 2010, pp. 4669 – 4674.

[5] M. Bühler, D. E. Koditschek, and P. Kindlmann, "A one degree of freedom juggler in a two degree of freedom environment," in *Proceedings of the International Workshop on Intelligent Robots*, Tokyo, Japan, 1988, pp. 91 – 97.

[6] R. Ronsse, P. Lefevre, and R. Sepulchre, "Rhythmic feedback control of a blind planar juggler," *IEEE Transactions on Robotics*, vol. 23, no. 4, pp. 790–802, 2007.

[7] P. Reist and R. D'Andrea, "Bouncing an unconstrained ball in three dimensions with a blind juggling robot," in *2009 IEEE International Conference on Robotics and Automation*, Kobe, Japan, May 2009, pp. 1774 – 1781.

[8] S. Haddadin, M. Weis, S. Wolf, and A. Albu-Schäffer, "Optimal control for maximizing link velocity of robotic variable stiffness joints," in *accepted to: IFAC World Congress*, 2011.

[9] J. Yamaguchi, D. Nishino, and A. Takanishi, "Realization of dynamic biped walking varying joint stiffness using antagonistic driven joints," in *IEEE Int. Conf. on Robotics and Automation (ICRA1998), Leuven, Belgium*, 1998, pp. 2022–2029.

[10] M. Okada, S. Ban, and Y. Nakamura, "Skill of compliance with controlled charging/discharging of kinetic energy," in *IEEE Int. Conf. on Robotics and Automation (ICRA2002), Washington, USA*, 2002, pp. 2455–2460.

[11] S. Haddadin, K. Krieger, and A. Albu-Schäffer, "Exploiting elastic energy storage for cyclic manipulation: Modeling, stability, and observations for dribbling," in *submitted to: IEEE Conference on Decision and Control*, Orlando, USA, 2011.

[12] K. Waldron and J. Schmiedeler, *Springer Handbook of Robotcis*, B. Siciliano and O. Khatib, Eds. Springer, 2005.

[13] K. H. Hunt and F. R. E. Crossley, "Coefficient of restitution interpreted as damping in vibroimpact," *Journal of Applied Mechanics*, vol. 42, pp. 440–445, 1975.

[14] C. C. de Wit and P. Tsiotras, "Dynamic tire friction models for vehicle traction control," in *Proceedings of the IEEE Conference on Decision and Control*, Phoenix, USA, 1999, pp. 3746 – 37 251.

[15] D. Gross, W. Hauger, J. Schröder, W. Wall, and J. Bonet, *Engineering Mechanics 2: Mechanics of Materials*. Heidelberg, Germany: Springer, 2011.

[16] S. V. Drakunov, "Sliding-mode observer based on equivalent control method," in *Proceedings of the 31st Contefence on Decision and Control*, Tuscon, USA, December 1992, pp. 2368 – 2369.

[17] D. Gross, W. Hauger, and J. Schröder, *Engineering Mechanics 1: Statics*. Heidelberg, Germany: Springer, 2009.